Ultrafast electron dynamics in GeSi nanostructures

S. A. Cavill, A. Potenza, and S. S. Dhesi
Diamond Light Source, Chilton, Didcot, Oxfordshire OX11 0DE, United Kingdom
(Received 3 October 2011; published 17 January 2012)

The relaxation dynamics of photoexcited hot carriers in Ge_xSi_{1-x} islands grown on Si(111)-(7 × 7) have been studied with the spatial and temporal resolution of time-resolved two-photon photoemission electron microscopy. The relaxation dynamics of the excited electronic states within the Ge-rich Ge_xSi_{1-x} dots and the surrounding Si-rich wetting layer are found to vary significantly below the conduction-band minimum. These differences are ascribed to faster hot-carrier-diffusion rates for the islands compared to those for the wetting layer.

DOI: 10.1103/PhysRevB.85.035421 PACS number(s): 68.37.Xy, 78.47.jd

I. INTRODUCTION

The explosive increase in the speed of nanoscale electronics has resulted in a huge effort to understand semiconductor carrier dynamics on ultrafast timescales. In this respect Ge/Si-based materials are potentially very promising for future device applications due to their enhanced optoelectronic properties, their ease of integration into existing microelectronic technologies,[1] and their ability to self-assemble into nanostructures. Quantum confinement offers a pathway to enhancing the optical performance of Si-based heterostructures, and GeSi materials are particularly important in this respect because there exists a strong relation between morphology and the optical and transport properties of the material.[2,3] Many new quantum-device concepts have recently been reported in the literature,[4,5] but several critical issues remain unresolved. These include morphology, uniformity, and compositional control.

The tetragonal deformation of the Ge epilayer, caused by the small lattice mismatch between Si and Ge, allows Ge to initially grow on Si in a layer-by-layer mode. Once a critical thickness is reached, the energy of the system can be lowered by the formation of three-dimensional (3D) islands, providing a simple and promising way to engineer quantum devices. However, the growth of defect-free coherent structures is essential in avoiding hot-carrier traps that affect recombination pathways and therefore quantum efficiencies. On the other hand, compositional homogeneity between individual nanostructures is crucial since small differences can considerably affect the electronic structure. Since these two issues largely determine the optoelectronic properties, it is vital to control and manipulate them. An important step in this direction is to use spectroscopic probes to understand the changing nature of the electronic structure as defects and composition evolve in the growth of nanostructures.

Recent work on relaxation dynamics has concentrated on the use of optical probes, such as time-resolved photoluminescence,[6] transient reflectivity,[7] or detection of the decay products,[8] to elucidate the various pathways and processes. Unfortunately, such probes do not directly measure the hot-carrier electronic distribution and are mainly restricted to bulk-material properties, rendering them of limited use for surface nanostructures. Probes which combine ultrafast optical pulses and surface sensitivity, such as second-harmonic generation (SHG),[9] five-wave mixing,[10] and other nonlinear methods,[11] have been developed but do not directly access the electronic structure. On the other hand, time-resolved two-photon photoelectron spectroscopy (TR-2P-PES)[12–16] combines ultrafast time-resolved spectroscopy with surface sensitivity. However, TR-2P-PES cannot resolve the spatially varying electron dynamics of inhomogeneous systems. A powerful method to overcome this issue is to combine TR-2P-PES with a photoemission electron microscope (PEEM) and use time-resolved two-photon photoemission electron microscopy (TR-2P-PEEM).[17–19] This combination allows surface morphology and structure to be studied with a resolution of <30 nm while simultaneously accessing hot-carrier dynamics on ultrafast time scales.

Here, we combine TR-2P-PES with the spatial resolution of a PEEM to study ultrafast relaxation dynamics from Ge_xSi_{1-x} islands grown on the Si(111)-(7 × 7) surface. The results demonstrate that the relaxation dynamics of the wetting layer (WL) are distinctly different compared to those of the Ge-rich nanostructured islands. The results are interpreted as differences in terms of hot-carrier-diffusion efficiencies.

II. EXPERIMENTAL METHODS

The experiments were performed in a UHV system operating at a base pressure of $<5 \times 10^{-10}$ mbar. Atomically clean Si(111)-(7 × 7) surfaces were prepared by extensive degassing of *B*-doped ($\rho = 0.1$ Ωcm) Si at 600 °C, followed by repeated flash annealing to 1200 °C. The surface crystallinity was verified by a sharp low-energy electron-diffraction (LEED) pattern characteristic of the (7 × 7) reconstruction. Low-energy electron microscopy (LEEM) of the surface at 41 eV revealed large terraces (∼400 nm). After stabilizing the sample temperature at 560 °C, Ge was deposited at a rate of 0.63 Å/minute. The growth mode was confirmed to be the Stranski-Krastanov type, i.e., the initial growth was layer-by-layer up to a critical thickness of 3–4 monolayers (MLs), followed by island nucleation.

TR-2P-PEEM was performed using the second harmonic (SH) and third harmonic (TH) of a mode-locked Ti:sapphire laser (repetition rate = 83 MHz and pulse length < 120 fs). A fraction of the SH ($\hbar\omega = 3.1$ eV) was used to excite (pump) the ground state into unoccupied intermediate states whilst the TH ($\hbar\omega = 4.6$ eV) was used to photoemit (probe) electrons from both the ground state and excited intermediate states. The probe pulse was delayed with respect to the pump pulse using a mechanical delay stage. The SH and TH beams were collinearly focused to a 50 μm spot incident at 73° with respect

 ©2012 American Physical Society

to the surface normal. The polarization of the pump and probe pulses could be set to an arbitrary state between the *s* and *p* polarizations.

Photoelectrons emitted over a large angular range (30°) were imaged using the PEEM. The energy resolution of the PEEM depends on the mode of operation. In *imaging mode*, the resolution is ~300 meV with a spatial resolution of 30 nm. In order to perform spectroscopy, a series of images was collected for varying photoelectron kinetic energies from which an energy-distribution curve (EDC) was generated, allowing spatially resolved TR-2P-PES. In the *analyzer mode* of operation, the energy-dispersive plane of the PEEM electron analyzer was used to capture an entire EDC. In this mode the PEEM was used to spatially average over the full field of view (FOV) and generated an EDC with a spectral resolution of ~200 meV.

III. RESULTS

Figure 1 shows a LEEM image of a 10-ML film of Ge grown on the Si(111)-(7 × 7) surface. At this coverage and growth temperature, large 3D islands are observed on top of the 3–4-ML wetting layer. Initially, islands nucleate as truncated tetrahedra with corners pointing in the ⟨112⟩ directions[20] due to the anisotropy of the growth rate in these directions. The wetting layer has a (5 × 5) reconstruction whilst the tops of the islands have (7 × 7) reconstructions with Ge-Si intermixing dependent on the growth temperature and base area.[21] As the islands evolve with increasing deposition, new facets are added, and dislocations are introduced to relieve the strain energy inside each island. Eventually, the largest structures exhibit a complex-rounded shape with mass depletion at the island centers. Similar to previous studies, individual 3D structures at different stages of evolution coexist on the surface.[20]

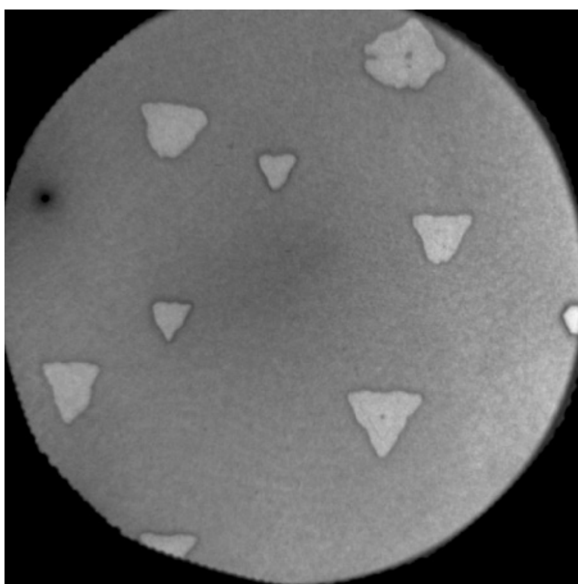

FIG. 1. LEEM image of a 10-ML film of Ge grown on a Si(111) surface. The field of view is 20 μm. The image was recorded with an incident electron energy of 8 eV.

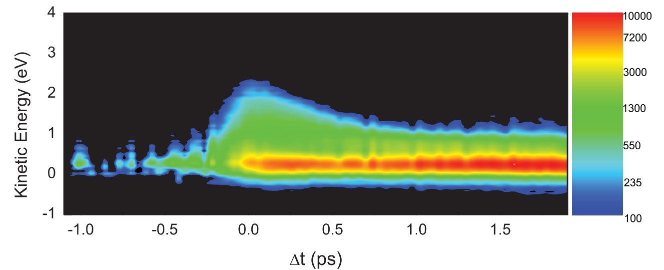

FIG. 2. (Color online) The change in photoemitted intensity (ΔI) as a function of Δt and E_K.

TR-2P-PES of the nanostructured surface was performed in analyzer mode (spatially averaged). Surface-band bending, due to the pinning of the Fermi level at surface states, has its own dynamical behavior under photoexcitation complicating the data. We therefore performed TR-2P-PES under flatband conditions. We first measured an EDC using only probe pulses and then again with the pump pulses at negative time delays and different intensities to obtain flatband conditions. This procedure resulted in identical spectra at moderate positive delays and at negative delays, showing that transient changes in the surface-band bending are small and that flatband conditions exist over all time scales. However, a two-photon component from the pump beam was also evident in all spectra measured. As this component was constant for a given pump-pulse intensity, it can be regarded as a background for spectra measured at positive time delays.

The dynamics of the excited-photoelectron distribution are shown in Fig. 2 in which a color-scale image maps the change in photoemitted intensity (ΔI) as a function of kinetic energy (E_K) and pump-probe delay (Δt). A spectrum recorded with $\Delta t = -2$ ps was subtracted from each spectrum to remove the background. In order to highlight important spectral features in the photoelectron-intensity map, vertical line scans can be extracted to yield time-resolved two-photon photoelectron spectra for several values of Δt as shown in Fig. 3. At $\Delta t = -1$ ps [Fig. 3(a)], ΔI is essentially zero, confirming that flatband conditions exist for all time scales and that the two-photon component from the pump is constant. During overlap of the pump and probe pulses ($\Delta t = 0$ ps), an increase in spectral weight occurs over a broad range of kinetic

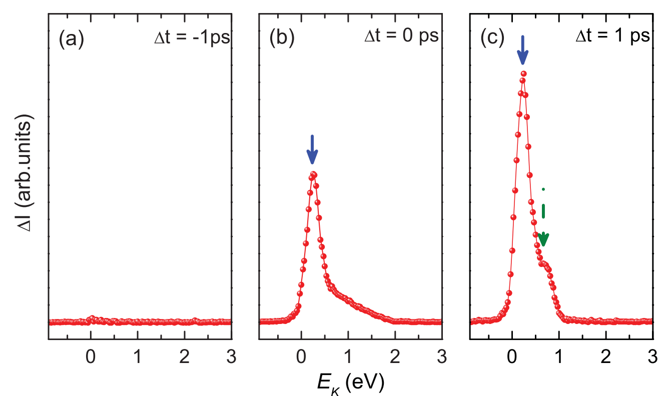

FIG. 3. (Color online) TR-2P-PE spectra measured with a *p*-polarised pump and probe pulses for (a) $\Delta t = -1$ ps, (b) $\Delta t = 0$ ps, and (c) $\Delta t = 1$ ps.

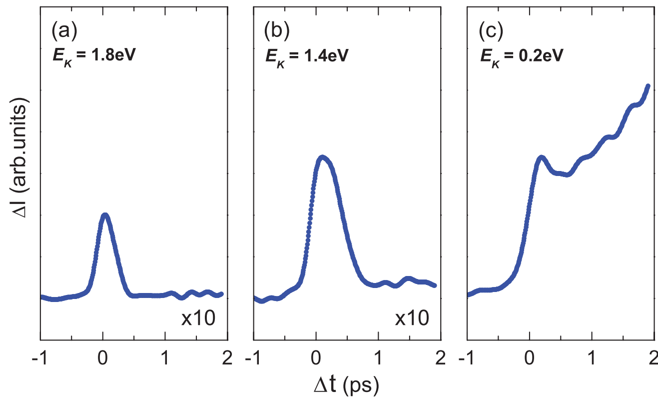

FIG. 4. (Color online) Transient change in the photoemission intensity measured for (a) $E_K = 1.8$ eV, (b) $E_K = 1.4$ eV, and (c) $E_K = 0.2$ eV.

energies with a maximum at $E_K \sim 0.22$ eV (blue arrow) as the pump pulse excites electrons into the unoccupied states. The broad photoemission component shows a fast temporal response for energies above $E_K = 1.6$ eV with a temporal profile essentially the same as the cross-correlation trace between pump and probe pulses. A similar effect was found previously and ascribed to a coherent two-photon process.[16] At $\Delta t = 1$ ps [Fig. 3(c)], two separate peaks can be resolved in the spectra. The low-energy peak with $E_K \sim 0.22$ eV [blue arrow in Fig. 3(c)] represents transient changes of the temporally occupied surface states. In addition, a peak forms around $E_K \sim 0.65$ eV [green dashed arrow in Fig. 3(c)].

The dynamics of the electrons excited into the unoccupied states can be followed using the photoemission intensity at fixed kinetic energies. Figure 4 shows horizontal line scans along the intensity map shown in Fig. 2 at several fixed kinetic energies. For a $E_K > 1.6$ eV [Fig. 4(a)], the dynamic response shows the same temporal profile as the cross correlation between pump and probe pulses as discussed earlier. However, for 1.2 eV $< E_K <$ 1.6 eV [Fig. 4(b)], the dynamic response shows a marked difference from the cross-correlation spectrum, implying photoemission from real short-lived intermediate states. At a $E_K = 0.2$ eV [Fig. 4(c)], a different set of dynamics is evident, characterised by an increasing photoemission intensity for $\Delta t > 500$ fs. The temporal response of the photoemission intensity at these intermediate-state energies therefore shows two time scales involved in the population of the unoccupied states. Initially, the pump beam photoexcites carriers into the intermediate states, evidenced by the fast initial rise in the TR-2P-PE intensity. However, a second process, which populates states on much slower time scales, is also present. This can be seen in Fig. 4(c) by the slow increase in photocurrent up to a Δt of 1.5 ps, which continues to rise up to 10 ps after the initial pump pulse.[22] For time scales longer than the pump pulse duration, the increase in intensity must involve population by the decay of carriers out of higher lying states. The time-dependent-photoemission intensity consequently reflects a set of complex dynamics involving excitation, scattering, and recombination processes.

TR-2P-PEEM was then performed using the imaging mode (spatially resolving) of the PEEM analyser. Figure 5 shows a PEEM image of the surface, measured with TH light, used for the spatially resolved measurements. A series of images was recorded as a function of Δt and E_K. Figure 6 shows the change in the TR-2P-PEEM intensity (ΔI), determined by integrating over a particular region of interest in Fig. 5. In Fig. 6 the blue curves represent the dynamics of the wetting layer (blue box in Fig. 5) whilst the red curves show the dynamics of the Ge_xSi_{1-x} nanoislands (red boxes in Fig. 5). The photoemission intensity at $\Delta t = 0$ ps for each kinetic energy has been normalized to unity.

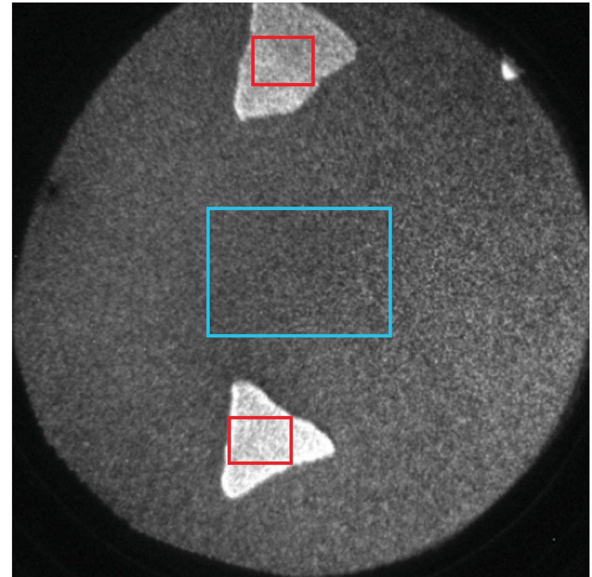

FIG. 5. (Color online) PEEM image of the Ge_xSi_{1-x} thin film recorded using $\hbar\omega = 4.6$ eV light. The FOV is 10 μm. The red (and blue) boxes represents the area from which spectra in Fig. 6 are derived for various photoelectron kinetic energies.

The dynamics of the islands and wetting layer show considerable differences for $E_K < 1.0$ eV, i.e., for intermediate-state energies within the band gap. For the islands, the surface-state dynamics ($E_K = 0.2$–0.6 eV) can be characterized by a large increase in intensity due to the pump beam followed by an additional component, giving rise to a shoulder in the spectra at $\Delta t \sim 500$ fs. These transiently occupied states decay rapidly to near-background intensity within 3 ps. The islands only show a longer relaxation time at $E_K = 0.2$ eV. The wetting layer, however, shows changes in intensity that resemble those shown in Fig. 4(c), recorded using the analyzer mode of the PEEM without spatial resolution. At kinetic energies below 0.6 eV, corresponding to photoemission from states within the band gap, two time scales are evident in the carrier dynamics. After the fast initial rise in intensity due to the pump, a slow increase in intensity over several picoseconds is followed by a slower decay of the photoemission intensity. In order to highlight the differences in the relaxation time as a function of E_K, the data in Fig. 6 are fitted to

$$\Delta I(t) = [A/w\sqrt{(\pi/2)}]\exp\{-2[(t-t_0)/w]^2\} + B[1-\exp(-t/\tau_1)]\exp(-t/\tau_2), \quad (1)$$

where w and t_0 are the Gaussian width and center, respectively, and τ_1 and τ_2 are the time constants for indirect population

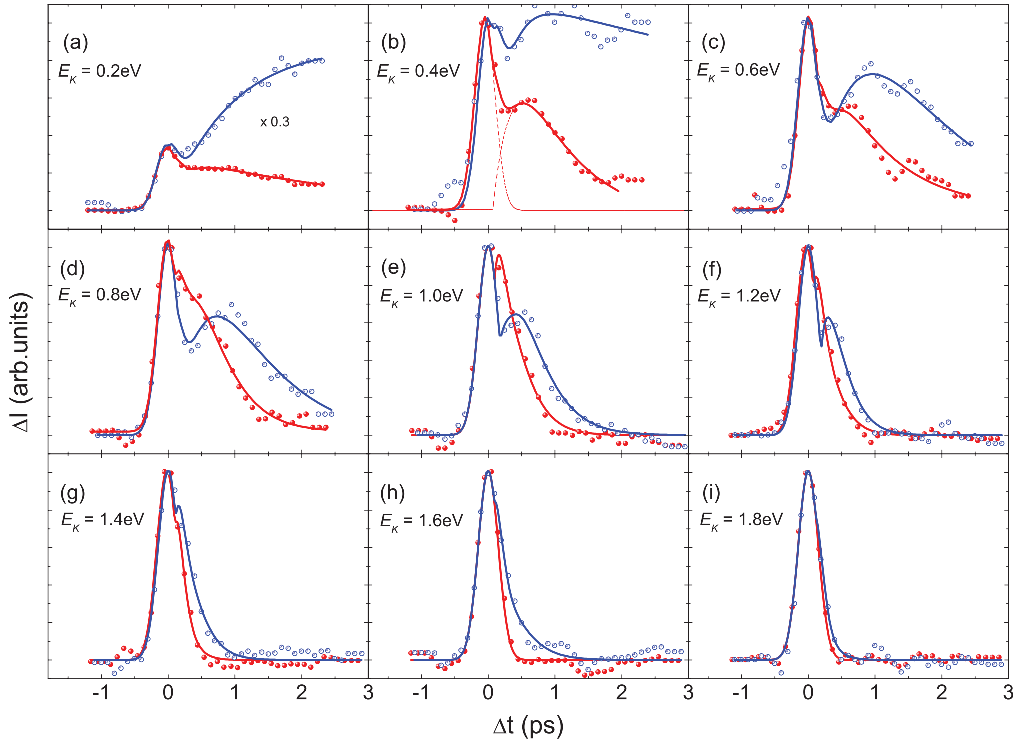

FIG. 6. (Color online) Transient changes in the photoemission intensity measured for the islands (red circles) and wetting layer (blue open circles) at kinetic energies of (a) 0.2 eV, (b) 0.4 eV, (c) 0.6 eV, (d) 0.8 eV, (e) 1.0 eV, (f) 1.2 eV, (g) 1.4 eV, (h) 1.6 eV, and (i) 1.8 eV. The solid lines represent fits according to Eq. (1). (b) The dashed lines show an example of the fitted Gaussian and exponential terms from Eq. (1).

into and relaxation out of the electronic states. A and B are constants of proportionality. The first term models the direct photon-pulse generation whilst the second term accounts for the temporal evolution of the indirect population (τ_1) and decay (τ_2) in the signal after the initial pulse as is shown implicitly in Fig. 6(b). The data from the islands in Fig. 6(i) are used to obtain parameters for the Gaussian generation term as it approximates accurately the cross correlation between the pump and probe pulses. The fitted Gaussian parameters are then used as constants for all other data. Table I shows the fitting parameter τ_2 (relaxation time) as a function of kinetic energy for the dots and wetting layer.

IV. DISCUSSION

The E_K of the photoemitted electrons is given by

$$E_K = \hbar\omega + E_{\text{CBM}} - \chi, \tag{2}$$

where $\hbar\omega$ is the probe-photon energy, E_{CBM} is the electronic energy relative to the conduction-band minimum (CBM), and

TABLE I. Decay parameter (τ_2) from fits to the data in Fig. 6.

Kinetic Energy (eV)	τ_2 (ps) [Dots]	τ_2 (ps) [WL]
0.2	3.0 ± 0.3	N/A
0.4	0.7 ± 0.1	11 ± 3
0.6	0.85 ± 0.08	0.88 ± 0.01
0.8	0.4 ± 0.2	0.66 ± 0.01
1.0	0.24 ± 0.08	0.32 ± 0.01

χ is the electron affinity. Here we assume that the conduction band offset in Ge/Si heterostructures, which depends on the composition and strain, is small and comparable to the energy resolution of the PEEM analyzer. In addition, the electronic structure of Ge_xSi_{1-x} is known to depend strongly on x.[23] However, since Ge and Si both have electron affinities of ~4 eV, the islands and wetting layer are also assumed to have an electron affinity of 4 eV over the whole range of x. Given the probe energy of $\hbar\omega = 4.6$ eV, photoemission from the CBM will result in a peak at a $E_K \sim 0.6$ eV. Therefore, the peak at a $E_K \sim 0.65$ eV for $\Delta t = 1$ ps in Fig. 3(c) is energetically consistent with photoemission from the CBM. The slight difference in the measured E_K is due to the hot-electron distribution near the CBM combined with the energy resolution of the PEEM electron analyzer. We note that, given the large angular acceptance of the PEEM and the fact that the CBM can be transferred to near one of the (7×7) unit cells as discussed in Ref. 16, momentum requirements also imply that the peak at a $E_K \sim 0.65$ eV can arise from states close to the CBM. However, it is important to establish if the photoemission process involves a direct transition into a final state ~4.6 eV above the CBM, a phonon-assisted indirect transition, or a transition into an evanescent final state induced by the surface photoelectric effect.[24] In order to resolve this issue, we measured the dependence of the $E_K \sim 0.65$ eV peak on the probe polarization. Recent studies have shown that, in Si, photoemission from the CBM at these photon energies can only be generated by p-polarised light.[24] A strong polarization dependence would then indicate a surface photoelectric effect that can induce photoemission

by exciting transiently populated electrons at the CBM into final states that are evanescent in nature. The results show[22] that the $E_K \sim 0.65$ eV peak decreases in intensity as the probe polarization is rotated from p to s, implying that this feature arises from the surface photoelectric effect.[24] Photoemission into evanescent final states would also explain the low intensity of the $E_K \sim 0.65$ eV peak, compared to the peak related to emission from the surface states, even though the density of states at the CBM should be considerably larger.

We next turn our attention to the spatially resolved data of Fig. 6. The electronic properties of both the (7×7) and (5×5) reconstructed Ge-covered surfaces are found to be qualitatively similar to that of the Si(111)-(7×7) surface.[25] In the absence of detailed electronic-structure calculations for Ge_xSi_{1-x}, we will interpret our results in terms of the known electronic structure of the Si(111)-(7×7) surface. Early TR-2P-PE results from Si(111)-(7×7) surfaces found gap-state lifetimes >10 ps[26] whilst more recent work demonstrated lower values of the surface-state lifetimes.[9,16] Our results are consistent with both, c.f., Table I, and indicate that the lifetime is strongly dependent on the intermediate-state energy. However, in Fig. 6 we observe clear differences in the dynamics of the islands and the wetting layer for $E_K < 0.8$ eV, i.e., for intermediate energies that correspond to states close to and below the CBM.

For the islands, the TR-2P-PE spectra shown in Fig. 6 are dominated by the direct population of surface states by the pump pulse. Photoemission and inverse photoemission[25] show that the Ge(7×7)-Si(111) surface bands are very similar in energy to those of the pure Si(111) surface. A direct transition between surface bands has been observed on the Si(111) surface[27] using a similar photon energy and was assigned to a transition from the $S3$ to $U2$ band. Accordingly, it is likely that the origin of the direct population by the pump in our data is the same as that of the Si(111) surface. A second increase in the photoemission intensity at delay times greater than the pump width and with subpicosecond decay times (τ_2), caused by the competition of decay into and out of these states, is also evident for $0.4 \text{ eV} < E_K < 1.6$ eV. Only at the lowest E_K does τ_2 increase significantly (see Table I). This is consistent with a distribution of states that allows carriers entering from the CBM to scatter progressively toward the Fermi level via the metallic surface-state bands. In metallic systems the carrier lifetime scales with the inverse square of the energy difference of the carrier with the Fermi level[28] so that the lifetimes increase as the hot carriers relax toward the Fermi level. Population feeding of these states by carriers decaying from high-lying states seems to be rather small, suggesting a weak coupling between the bulk and the surface states.[9]

The wetting layer also shows a fast increase in population on the time scale of the pump beam, but now for kinetic energies corresponding to states around and below the CBM (<0.8 eV), the signal is followed by a large and relatively slow rise in intensity on time scales longer than that of the pump. This can only be due to considerable population feeding from carriers relaxing out of higher lying states. Evident from the data (Fig. 6 and Table I) is that the decay out of these states occurs on longer time scales than does that of the corresponding kinetic energies of the islands. The main reason that TR-2P-PE spectra show such dramatic differences between the islands and the wetting layer is most likely related to the diffusion of conduction electrons away from the surface into the bulk after the absorption of the ($\hbar\omega = 3$ eV) pump pulse.

Since the absorption depth at the pump energy ($\hbar\omega = 3$ eV) is 15 nm (Ge) and 122 nm (Si), which is reduced to $\sim$5 nm (Ge) and $\sim$5 nm (Si) at the probe energy ($\hbar\omega = 4.6$ eV), the hot-carrier-concentration gradient near the surface is much higher after absorption of the pump for the Ge-rich islands than for the Si-rich wetting layer. In addition, the thickness of the wetting layer ($\sim$3 MLs) implies that the probe beam is predominantly sensitive to the Si substrate whilst for the Ge-rich islands it is only sensitive to the islands. Following a similar analysis,[26] the time for the average carrier to diffuse a distance equal to the absorption depth of the probe is found to be greater for the Si-rich wetting layer than the Ge-rich islands due to the weaker carrier-concentration gradient. It therefore seems reasonable that for the wetting layer, the rate at which carriers enter the surface states via the conduction band will be higher due to the slower rate of diffusion away from the surface. The dynamics are therefore governed not only by the decay channels at the bottom of the surface band but also by the electron flow into it. Similar effects have also been reported by Tanaka *et al.*[29] who found wavelength-dependence dynamics of the surface states and CBM related to the wavelength dependence in the carrier gradient.

V. SUMMARY

We have studied the excited-state electron dynamics in Ge_xSi_{1-x} islands using the spatial resolution of PEEM combined with two-photon photoemission (2P-PE) spectroscopy. We found that a pronounced peak in the spatially averaged 2P-PE can be attributed to photoemission from transiently occupied states near the conduction-band minimum. Therefore, time-resolved 2P-PE can probe hot-electron dynamics from both surface and bulk states simultaneously. The spatially resolved results reveal that the surface states of the Si-rich wetting layer have a different set of dynamics than that of the Ge-rich Ge_xSi_{1-x} islands. This has been interpreted as a difference in the population feeding of the surface states between the islands and the wetting layer due to the faster diffusion of conduction electrons away from the surface for the former. Future studies involving excitation at different wavelengths should help to further clarify the distinct role of carrier-diffusion dynamics in localized structures.

ACKNOWLEDGMENT

We would like to thank Richard Mott for his technical assistance.

[1] I. Berbezier, A. Ronda, and A. Portavoce, J. Phys.: Condens. Matter **14**, 8283 (2002).
[2] D. J. Paul, Adv. Mater. (Weinheim, Ger.) **11**, 191 (1999).
[3] L. Vescan, M. Goryll, T. Stoica, P. Gartner, K. Grimm, O. Chretien, E. Mateeva, C. Dieker, and B. Holländer, Appl. Phys. A: Mater. Sci. Process. **71**, 423 (2000).

[4]G. Dehlinger, L. Diehl, U. Gennser, H. Sigg, J. Faist, K. Ensslin, D. Grützmacher, and E. Müller, Science **290**, 2277 (2000).
[5]Jifeng Liu, Mark Beals, Andrew Pomerene, Sarah Bernardis, Rong Sun, Jing Cheng, Lionel C. Kimerling, and Jurgen Michel, Nat. Photonics **2**, 433 (2008).
[6]F. Pulizzi, A. J. Kent, A. Patanè, L. Eaves, and M. Henini, Appl. Phys. Lett. **84**, 3046 (2004).
[7]T. Guenther, C. Lienau, T. Elsaesser, M. Glanemann, V. Martin Axt, T. Kuhn, S. Eshlaghi, and A. D. Wieck, Phys. Rev. Lett. **89**, 057401 (2002).
[8]A. V. Akimov, S. A. Cavill, A. J. Kent, N. M. Stanton, T. Wang, and S. Sakai, J. Phys.: Condens. Matter **14**, 3445 (2002).
[9]M. Mauerer, I. L. Shumay, W. Berthold, and U. Höfer, Phys. Rev. B **73**, 245305 (2006).
[10]T. Meier, M. Reichelt, S. W. Koch, and U. Höfer, J. Phys.: Condens. Matter **17**, S221 (2005).
[11]C. K. Chen, A. R. B. de Castro, Y. R. Shen, and F. DeMartini, Phys. Rev. Lett. **43**, 946 (1979).
[12]For a review of the subject see: R. Haight, Surf. Sci. Rep. **21**, 275 (1995).
[13]J. R. Goldman and J. A. Prybyla, Phys. Rev. Lett. **72**, 1364 (1994).
[14]K. I. Shudo, S. Takeda, and T. Munakata, Phys. Rev. B **65**, 075302 (2002).
[15]S. Jeong, H. Zacharias, and J. Bokor, Phys. Rev. B **54**, R17300 (1996).
[16]T. Ichibayashi and K. Tanimura, Phys. Rev. Lett. **102**, 087403 (2009).
[17]A. Kubo, K. Onda, H. Petek, Z. Sun, Y. S. Jung, and H. Koo Kim, Nano Lett. **5**, 1123 (2005).
[18]M. Munzinger, C. Wiemann, M. Rohmer, L. Guo, M. Aeschlimann, and M. Bauer, New J. Phys. **7**, 68 (2005).
[19]O. Schmidt, M. Bauer, C. Wiemann, R. Porath, M. Scharte, O. Andreyev, G. Schonhense, and M. Aeschlimann, Appl. Phys. B: Lasers Opt. **74**, 223 (2002).
[20]N. Motta, J. Phys.: Condens. Matter **14**, 8353 (2002).
[21]F. Ratto, F. Rosei, A. Locatelli, S. Cherifi, S. Fontana, S. Heun, P. Szkutnik, A. Sgarlata, M. De Crescenzi, and N. Motta, J. Appl. Phys. **97**, 043516 (2005).
[22]S. A. Cavill *et al.* (unpublsihed).
[23]See [http://www.ioffe.ru/SVA/NSM/Semicond/SiGe/bandstr.html], and references therein; N. Fraj, I. Saïdi, S. Ben Radhia, and K. Boujdaria, J. Appl. Phys. **102**, 053703 (2007).
[24]T. Ichibayashi and K. Tanimura, Phys. Rev. B **75**, 235327 (2007).
[25]P. Martensson, W. Ni, G. V. Hansson, J. M. Nicholls, and B. Reihl, Phys. Rev. B **36**, 5974 (1987).
[26]M. W. Rowe, H. Liu, G. P. Williams Jr., and R. T. Williams, Phys. Rev. B **47**, 2048 (1993).
[27]K. I. Shudo, S. Takeda, and T. Munakata, Phys. Rev. B **65**, 075302 (2002).
[28]I. Campillo, V. M. Silkin, J. M. Pitarke, E. V. Chulkov, A. Rubio, and P. M. Echenique, Phys. Rev. B **61**, 13484 (2000).
[29]S. Tanaka, T. Ichibayashi, and K. Tanimura, Phys. Rev. B **79**, 155313 (2009).